Virtual

IUTAM International Union of Theoretical and Applied Mechanics

25th International Congress of Theoretical and Applied Mechanics

August 22-27, 2021

BOOK OF ABSTRACTS

Editor: **Alberto Corigliano**

ISBN number: **978 -83-65550-31-6**

under the auspices of

POLITECNICO MILANO 1863

UNIVERSITÀ DI PAVIA

www.ictam2020.org

ICTAM Milano 2020+1 Virtual

BENDING OF FLEXIBLE FIBERS IN SHEAR FLOW IS OFTEN DRIVEN BY THEIR ENDS

Pawel J. Zuk*[1,2], Agnieszka M. Slowicka[1], Maria L. Ekiel-Jezewska[1], and Howard A. Stone[2]
[1]Institute of Fundamental Technological Research, Polish Academy of Sciences, Warsaw, Poland
[2]Department of Mechanical and Aerospace Engineering, Princeton University, Princeton, USA

Summary We present a numerical study of the dynamics of an elastic fiber in shear flow. The simulations are done in the bead-spring framework including hydrodynamic interactions in two theoretical schemes: the Generalized Rotne-Prager-Yamakawa model and a multipole expansion corrected for lubrication. We focus on the evolution of an initially straight fiber oriented in the flow direction. In the simulations fibers have aspect ratio from 20 to 200 and various bending stiffnesses: fiber shape vary from highly bent to straight. We discover variations of the fiber shapes and dynamics that follow powers, e.g. the fiber curvature changes as fiber stiffness to the power -1/4, and show that time scales of fiber rotation (length dependent) and fiber bending (stiffness dependent, length independent) determine the fiber motion. The numerical results are further supported with an analytical elastica model.

INTRODUCTION

The behavior of fibers immersed in the shear flow is a phenomena studied experimentally [1, 2], theoretically and numerically [3, 4, 5] in the context of fundamental understanding and technological applications of fibrous materials [6]. Here we focus on the dynamics of a single, flexible fiber that is initially stretched in the direction of the shear flow. We perform numerical simulations for different lengths and stiffnesses using a bead-spring model of a fiber. The results demonstrate that for a finite aspect ratio the fiber end effects are important to understand the shape of the fiber and its evolution, at least in part because they introduce a separate time scale.

METHODS

In simulations we use the bead-spring model common to studies of the dynamics of suspensions in the regime of small Reynolds numbers [7]. The fiber consists of N beads (with diameter d, position $\mathbf{R}_i$) that are interacting with stretching and bending potentials, and the fiber is placed in a fluid of viscosity η undergoing a shear flow with shear rate $\dot{\gamma}$. Between every two consecutive beads in the chain we impose the FENE stretching potential with equilibrium distance d between the bead centers and maximum stretch $0.1d$, which has a stretching resistance large enough to mimic an inextensible structure. Indeed, the observed changes in the fiber length does not exceed 0.1% of the total fiber length. The bending potential E_{bi} acts between every three consecutive beads $(i-1, i, i+1)$ restricting the shape of the fiber. We used harmonic $E_{bi} = \frac{A'}{2}(\theta_i - \pi)^2$ and cosine $E_{bi} = A'(1+\cos(\theta_i))$ bending potentials, where $\theta_i = \text{arc cos}\left(\frac{(\mathbf{R}_{i-1}-\mathbf{R}_i)\cdot(\mathbf{R}_{i+1}-\mathbf{R}_i)}{|\mathbf{R}_{i-1}-\mathbf{R}_i||\mathbf{R}_{i+1}-\mathbf{R}_i|}\right)$. The dimensionless bending stiffness $A = A'/(\pi\eta\dot{\gamma}d^3)$ and the number of beads N are treated as parameters. We used two different hydrodynamic interactions (HI) models: the Generalized Rotne-Prager-Yamakawa (GRPY) [8] and the Hydromultipole algorithm [4] based on the multipole expansion corrected for lubrication. In case of the GRPY approximation, to prevent sphere overlap, spheres that are more distant than nearest neighbors interact with the repulsive part of the Lennard-Jones potential. We focus here on GRPY with harmonic bending potential.

RESULTS

The quantity that we investigate in detail is the maximum curvature κ over the fiber length at every instant of time. For each consecutive three beads $(i-1, i, i+1)$ the local curvature κ_i is the inverse of a radius of a circle circumscribed on points $\mathbf{R}_{i-1}, \mathbf{R}_i, \mathbf{R}_{i+1}$. For each time we take the maximum of κ_i over all nearest neighbor triplets in the fiber and denote this quantity κ. An example of κ as a function of time is shown in Figure 1A. We will focus on two characteristic features of $\kappa(t)$: a time τ_b that is needed for a fiber to bend (interval from the beginning of the simulation to the rapid increase in κ) and maximum of κ observed over time that we will denote κ_b. In Figure 1B the corresponding shapes of the fiber are shown during the time instances marked in Figure 1A.

The maximum bending curvature κ_b as a function of dimensionless bending stiffness A is presented in Figure 1C. Generically a fiber of a given length will have three distinct behaviors as a function of A. First, in the regime of the smallest A, κ_b is limited primarily by the excluded volume of the beads. Second, in the regime of the intermediate A, κ_b is best described by the local bending. In this regime the shape follows the scaling law $\kappa_b \propto A^{-1/4}$ that can be understood from the interplay between the shear flow and elasticity, as we demonstrate with the elastica model. Third, in the regime of large A the fiber bends globally leaving the scaling law typical for the second regime. The transition between the second and third regimes depend on N and for larger N occurs at larger A.

*Corresponding author. E-mail: pzuk@ippt.pan.pl.

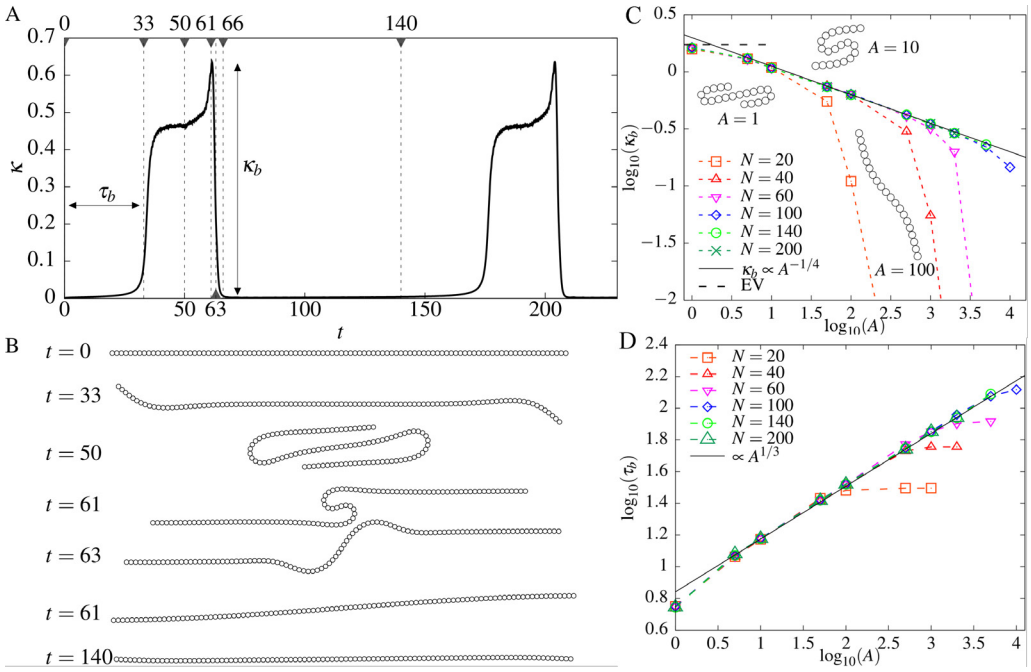

Figure 1: Flexible fiber in the shear flow calculated with the GRPY model. (A) The maximum curvature chosen over the fiber length as a function of time for the fiber of length $N = 100$ and $A = 100$. (B) Fiber shape corresponding to the time instants marked in the panel A and the same simulation. (C) The maximum curvature κ_b that a fiber reaches during simulation as a function of A for different N. The EV denotes the curvature limit from the excluded volume of the spheres. In the insets the characteristic bent shapes of the fiber with $N = 20$ are shown. (D) The bending time τ_b as a function of A and N.

Another aspect of the transition between the second and third regimes of fiber bending arises from the detailed inspection of the bending times τ_b. In Figure 1D we show τ_b as a function of A for different N. Again, for a given fiber length we can distinguish three regimes: regime of small A, regime of intermediate A ($\tau_b \propto A^{1/3}$) and regime of large A (τ_b saturates). To justify the slope in Figure 1D we use the elastica model with an additional assumption: at the fiber end a constant hydrodynamic force is present. It is perpendicular to the fiber direction and oriented as the rotational component of the shear flow. This assumption is justified by the results obtained from the bead-spring approach.

The τ_b does not depend on the fiber length in the low and intermediate regimes of A (owing to the local nature of bending), however the transition between the local and global bending does depend on N. This can be understood from a competition of the two time scales present in the system. The time scale τ_r that a straight and stiff fiber needs to perform a quarter of periodic rotation in the shear flow and the time scale τ_b that the fiber end needs to bend from the stretched, flow aligned configuration. The behavior $\tau_r \propto N$ and its values are visible as saturation times in Figure 1D. Furthermore, using the τ_b the phase space of the shapes of elastic fiber evolving in the plane of shear flow can be explained.

ACKNOWLEDGEMENTS

We acknowledge a partial support of project ITHACA (nr PPI/APM/2018/1/00045/U/001) founded by Polish National Agency for Academic Exchange.

References

[1] Forgacs O. L., Mason S. G. Particle motions in sheared suspensions: IX. Spin and deformation of threadlike particles. *J. Coll. Sci.* **14(5)**:457-472, 1959.
[2] Perazzo A, Nunes J. K., Guido S., Stone H. A. Flow-induced gelation of microfiber suspensions. *P. Natl. Acad. Sci. USA* **114(41)**:E8557–E8564, 2017.
[3] Tornberg A.-K., Shelley M. J. Simulating the dynamics and interactions of flexible fibers in Stokes flows. *J. Comput. Phys.*, **196(1)**:8–40, 2004.
[4] Słowicka A. M., Wajnryb E., and Ekiel-Jeżewska M. L. Dynamics of flexible fibers in shear flow. *J. Chem. Phys.* **143(12)**:124904, 2015.
[5] Słowicka A. M., Stone H. A., Ekiel-Jeżewska M. L. Flexible fibers in shear flow approach attracting periodic solutions. *Phys. Rev. E* accepted, 2020; https://arxiv.org/abs/1905.12985.
[6] Du Roure O., Lindner A., Nazockdast E. N., Shelley M. J. Dynamics of flexible fibers in viscous flows and fluids. *Annu. Rev. Fluid Mech.* **51**:539–572, 2019.
[7] Gruziel M., Thyagarajan K., Dietler G., Stasiak A., Ekiel-Jeżewska M. L., Szymczak P. Periodic motion of sedimenting flexible knots. *Phys. Rev. Lett.* **121**:127801, 2018.
[8] Wajnryb E., Mizerski K. A., Zuk P. J., Szymczak P. Generalization of the RotnePragerYamakawa mobility and shear disturbance tensors. *J. Fluid Mech.* **731**, 2013.